

RSC Advances



This is an *Accepted Manuscript*, which has been through the Royal Society of Chemistry peer review process and has been accepted for publication.

Accepted Manuscripts are published online shortly after acceptance, before technical editing, formatting and proof reading. Using this free service, authors can make their results available to the community, in citable form, before we publish the edited article. This *Accepted Manuscript* will be replaced by the edited, formatted and paginated article as soon as this is available.

You can find more information about *Accepted Manuscripts* in the [Information for Authors](#).

Please note that technical editing may introduce minor changes to the text and/or graphics, which may alter content. The journal's standard [Terms & Conditions](#) and the [Ethical guidelines](#) still apply. In no event shall the Royal Society of Chemistry be held responsible for any errors or omissions in this *Accepted Manuscript* or any consequences arising from the use of any information it contains.

Cite this: DOI: 10.1039/c0xx00000x

www.rsc.org/xxxxxx

ARTICLE TYPE

Photoluminescence Quenching and Electron Transfer in CuInS₂/ZnS Core/Shell Quantum Dot and FePt Nanoparticle Blend Films

Jie Hua,^{a,b} Haibo Cheng,^a Xi Yuan,^a Yan Zhang,^a Mei Liu,^a Xiangdong Meng,^a Haibo Li^{*a,b} and Jialong Zhao^{*a}

Received (in XXX, XXX) Xth XXXXXXXXX 20XX, Accepted Xth XXXXXXXXX 20XX
DOI: 10.1039/b000000x

The photoluminescence (PL) quenching of CuInS₂/ZnS quantum dots (QDs) in blend films with FePt magnetic nanoparticles (MNs) was studied by steady-state and time-resolved PL spectroscopy. ZnS shell-coated CuInS₂ QDs having various Cu/In molar ratios were synthesized via a hot-injection method. The PL peak of the QDs with enlarged band gap was varied from 680 to 610 nm by decreasing the Cu/In ratio. The highest PL quantum yield of 44% was obtained for CuInS₂/ZnS QDs with an optimum Cu/In ratio of 1/6. The decrease in PL intensity and lifetime was observed in the blend films of CuInS₂/ZnS QDs and FePt MNs with different concentration, demonstrating that electron transfer occurred from CuInS₂ QDs to FePt MNs. Moreover, the rate and efficiency of electron transfer as a function of the concentration ratio of FePt MNs to CuInS₂ QDs and temperature were obtained. It was found that electron transfer rate significantly increased with increasing the FePt MN concentration and the temperature. Therefore, the experimental results indicated electron transfer-induced PL quenching in CuInS₂ QD and FePt MN blend films should be considered in designing the structure of magnetic-fluorescent nanocomposites for realizing their highly efficient PL.

Introduction

Magnetic-fluorescent nanocomposites have attracted intense attentions because they can integrate several functional materials with different properties such as optical, magnetic, and electronic properties into one kind of multifunctional nanocomposites, which afford great promise for fluorescence detection, enhanced magnetic resonance imaging, selective magnetic separation, information storage, and so on.¹⁻³ In searching for imaging agent, semiconductor quantum dots (QDs) have drawn much attention because their optical properties depend critically on the particle size, composition, and surface chemistry.⁴⁻⁶ Great efforts have been devoted to the combination of FePt or Fe₃O₄ magnetic nanoparticles (MNs) with various luminescent QDs, such as FePt-CdS,^{6,7} Fe₃O₄-CdSe,^{8,9} and FePt-CdSe.¹⁰ These nanocomposites retain the superparamagnetic property of MNs with the luminescence properties of QDs. The use of QDs and MNs for in vitro and in vivo imaging in biology and medicine becomes one of the most competitive fields in modern nanoscience. However, most of the QDs are cadmium-containing materials, which make the future applicability of these nanocrystals doubtful and give the concerns for potential health and environmental risks. Therefore, it is necessary to find novel QDs to enhance the application for these multifunctional nano-materials.

Recently, ternary CuInS₂ QDs are considered to be one of the most promising candidates to replace cadmium-based II-VI QDs for biomedical research, because they do not contain highly toxic

element and have size- and composition-tunable PL from the near infrared (direct band gap (1.53 eV) of the bulk CuInS₂) to the visible region.¹¹⁻¹⁵ Chang group reported the synthesis of magnetic-fluorescent SiO₂ nanohybrids, which were composed of CuInS₂/ZnS QDs and Fe₃O₄ MNs.¹⁶ The nanohybrids could provide more efficient assistance of drug delivery into tumor cells for suppressing the growth of MCF-7 breast cancer cells. On the other hand, compared with Fe₃O₄, FePt alloy MNs have high anisotropy of 7×10^7 erg/cm⁻³ and high chemical stability. Therefore, it is expected that the hybrid nanostructures composed of CuInS₂ QDs and FePt MNs would be excellent magnetic-fluorescent nanocomposites. In order to better apply them in the biological field, the CuInS₂ QDs are needed to exhibit high efficiency photoluminescence (PL). Previous works have reported CuInS₂ QDs with tunable peak emissions and high PL quantum yields (QYs) by adjusting the cation composition or the QDs sizes.^{14, 17-19} Besides, the PL QYs of CuInS₂ QDs would be obviously enhanced after surface coating of ZnS shells because the binary ZnS layers can passivate the dangling bonds at the QDs surface, effectively removing the nonradiative intragap trap states associated with surface defects.^{18, 20}

Significant PL quenching has been observed in magnetic-fluorescent nanocomposites. The PL quenching processes are usually reflected by the change in fluorescent properties of the QDs such as the PL intensity and lifetime. In this work, the CuInS₂/ZnS core/shell QDs with various Cu contents in the raw material solution were synthesized using fast-injection approach. The PL properties of CuInS₂/ZnS QDs in FePt MN and

CuInS₂/ZnS QD blend films were studied by steady-state and time-resolved PL spectroscopy to understand PL quenching mechanism of the QDs. Further the effect of the concentration ratio of FePt MNs to CuInS₂ QDs and temperature on electron transfer processes between CuInS₂ QDs and FePt MNs was also analyzed.

Experimental section

Materials. Zinc acetate (Zn(OAc)₂, 99.99%), copper acetate (Cu(OAc)₂, 99.99%), indium acetate (In(OAc)₃, 99.99%), Iron (III) acetylacetonate (Fe(acac)₃, ≥ 99.9%), Platinum (II) acetylacetonate (Pt(acac)₂, 97%) sulfur powder (S, 99.99%), dodecanethiol (DDT, 99.9%), oleic acid (OA, ≥99%) oleylamine (OAm, 97%), 1-octadecene (ODE, 90%), and 1,2-hexadecanediol (90%) were purchased from Aldrich. All chemicals were used without further purification.

CuInS₂/ZnS Core/Shell QDs Synthesis. A typical synthesis process of CuInS₂/ZnS core/shell QDs was described as follows: Cu(OAc)₂, In(OAc)₃, 0.2 mL OA, 0.5 mL DDT, and 5 mL ODE were loaded into 50 mL of three-neck flask and degassed at 120 °C for 1 hour at this temperature, backfilled with Ar. Then the mixture was heated up to 150 °C and S precursor (obtained by dissolving 0.3 mmol sulfur in 1 mL OAm) was injected rapidly into the flask to form CuInS₂ nanoclusters. After 20 min, Zn precursor (0.3 mmol Zn(OAc)₂ dissolved in 0.5 mL OAm and 1.5 mL ODE) was introduced into the reaction solution. Followed this, the temperature of the mix solution was raised to 230 °C and kept at the temperature for 30 min to coat CuInS₂ cores with a ZnS shell. The CuInS₂ cores with different Cu/In ratios were obtained when the Cu/In precursor molar ratio was varied with 1/1, 1/3, and 1/6. The obtained CuInS₂/ZnS core/shell QDs were assigned as QD1, QD2 and QD3, respectively, and all other variables were remained constant. The QDs were precipitated by adding methanol into toluene solution and purified at least four times. The collected QDs were dispersed into chloroform for the subsequent measurement.

FePt MNs Preparation. 0.5 mmol of Pt(acac)₂, 0.5 mmol of Fe(acac)₃, 4 mmol of OA, 4 mmol of OAm, and 10 mL 1,2-hexadecanediol were added into a 25 mL three-neck flask under gentle Ar flow. The flask was heated to 160 °C and maintained for 15 min at this temperature to ensure the dissolution of Pt(acac)₂ and Fe(acac)₃. Then the solution was heated to 240 °C and kept at this temperature for 30 min. A black product was precipitated by adding ethanol and separated by centrifugation. The dispersion/precipitation procedure was repeated three times. Finally, the FePt MNs were dispersed in toluene.

Preparation of CuInS₂ QD/FePt MN Blend Films. Appropriate amount CuInS₂/ZnS QDs solution was added by a micropipette to 40 μL of FePt MNs solution (40 μM), then the mix solution were dropped or spin-coated onto cleaned silicon substrates. The blend films were obtained by changing the QDs solution (30 μM) concentration with 20, 40, 80, and 200 μL. These films were assigned as FePt MN/CuInS₂ QD volume ratio of 2.0, 1.0, 0.5, and 0.2, respectively.

Characterization. The X-ray diffraction (XRD) pattern of the as-prepared samples was recorded using a Rigaku D/max-2500 diffractometer with Cu Kα radiation at room temperature. The transmission electron microscope (TEM) and high-resolution

TEM images were recorded using a JEM-2100 electron microscope. The QDs dispersed in chloroform were dipped on carbon coated copper grids. Surface topography of films were analyzed by Agilent 5500 atomic force microscopy (AFM). The energy dispersive X-ray spectroscopy (EDX) for the elemental analysis of the QDs was performed by using JSM-7800F field emission scanning electron microscope (FE-SEM). Steady-state PL spectra, PL QYs, and time-resolved PL spectra were measured by a Horiba Jobin Yvon Fluorolog-3 with a QYs accessory and a time-correlated single-photon counting (TCSPC) spectrometer. The continuous excitation source was a 150 W ozone-free xenon arc-lamp. A pulsed xenon lamp or Nano-LED (N-405L) was utilized as the excitation source for the PL decay measurement. The film samples were mounted in a Janis VPF-800 vacuum liquid nitrogen cryostat with a controllable temperature region from 80 to 300 K, during the entire measurement. The magnetic property of the FePt MNs was measured with Lake Shore (M-7407) vibrating sample magnetometer (VSM).

Results and discussion

Fig. 1 shows the UV-visible absorption and normalized PL spectra of CuInS₂/ZnS core/shell QDs along with different Cu/In ratios. The CuInS₂/ZnS QDs exhibit a large Stokes shift of about 390 meV between their optical band gaps and the corresponding emission peaks. It has been demonstrated that a large Stokes-shift of I-III-VI QDs such as CuInS₂ can be ascribed to the presence of intrinsic defects states in the band gap, such as V_{Cu}, V_S, and In_{Cu}. Thus, the QDs only exhibit defect-related broad emissions instead of the band-to-band (exciton) emission.²¹

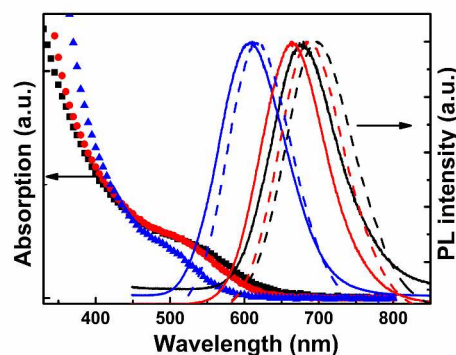


Fig. 1 UV-visible absorption and normalized PL spectra of CuInS₂/ZnS QDs in chloroform (solid line) and films on Si substrates (dashed line) with various Cu/In molar ratios of 1:1 (black line), 1:3 (red line), and 1:6 (blue line).

Both the absorption and emission spectra shift to short wavelength with decreasing the Cu/In molar ratio from 1/1 to 1/6. A broad absorption band for all the QDs is observed together with an absorption tail at the long wavelength side, because each ternary CuInS₂ QDs may vary in size, geometry, and stoichiometry. The PL peak shifts from 680 to 610 nm, having the full width at half maximum (FWHM) of about 104 nm. The PL QYs of CuInS₂/ZnS core/shell QDs were determined to be 15, 31, and 44 % for the QDs with Cu/In molar ratio of 1/1, 1/3, and 1/6, respectively. The results indicate the CuInS₂/ZnS core/shell QDs with different PL wavelength and QYs could be obtained by

changing the Cu/In ratio. The normalized PL spectra of QD films are shown in Fig. 1. It can be seen that the PL peak of QDs

obviously shift to red, which results from the energy transfer in closely packed QDs.

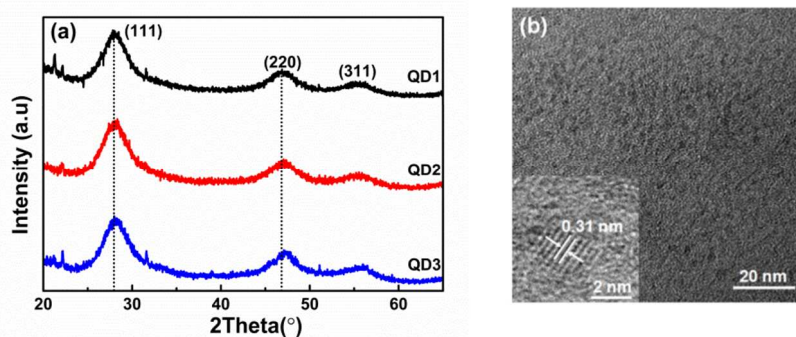


Fig. 2 (a) XRD patterns of CuInS₂/ZnS core/shell QDs with different Cu/In ratio. (b) The TEM image of QD3 with Cu/In ratio of 1/6. A high resolution TEM image of QD3 is shown in the inset.

The XRD patterns of as-synthesized CuInS₂/ZnS core/shell QDs are shown in Fig. 2(a). The patterns for the CuInS₂/ZnS QDs show the characteristic peaks of the zinc blende (cubic) structure, similar to those reported previously.^{21, 22} It can be seen that the FWHM of XRD diffraction peaks for samples are almost the same, indicating the sizes of the all samples are similar. The diffraction peak of the CuInS₂/ZnS QDs shifts to larger angles with decreasing the Cu/In ratio, which is consistent with the smaller In³⁺ ($r=0.094$ nm) cationic radius than those of Cu⁺

($r=0.100$ nm). The composition of the QDs was estimated by EDX [Table S1†]. The Cu/In molar ratios of the obtained QDn ($n=1-3$) were determined to be 1.13, 0.83, and 0.67, respectively. Their sizes are about 3.1 nm estimated from the TEM image as shown in Fig. 2(b). The shell thickness is estimated to be about 1 monolayer (ML) by using one ML ZnS (0.31 nm) on the basis of the respective compounds.²³ The high resolution TEM image exhibits clear lattice fringes as shown in the inset of Fig. 2(b), which suggests the highly crystalline nature.

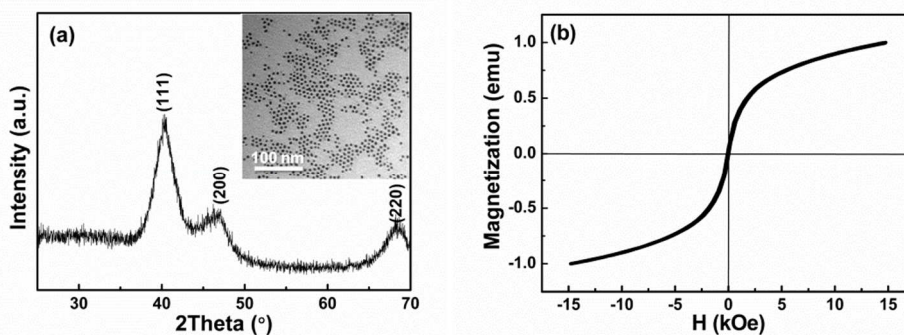


Fig. 3 XRD pattern (a) and VSM (b) of FePt MNs. The TEM image is shown in the inset of (a).

Fig. 3 shows the XRD pattern and VSM of the obtained FePt MNs. The corresponding TEM image is shown in the inset of Fig. 3(a). It can be seen that the as-prepared FePt MNs have chemically disordered fcc structure. The FePt MNs are uniform spherical-shaped particles and the size of the particles is about 4 nm. The room-temperature magnetic hysteresis curve of FePt MNs exhibits superparamagnetism at room temperature. No PL is observed in FePt MNs under excitation of 405 nm.

In order to understand the PL quenching of CuInS₂/ZnS core/shell QDs in CuInS₂-FePt system, the colloidal CuInS₂/ZnS QDs were mixed with FePt MNs and deposited as thin films. Fig. S1† shows the TEM and AFM images for CuInS₂-FePt deposited films from mixed colloids with various concentrations of FePt MNs, respectively, confirming the formation of blend films for FePt MNs and CuInS₂/ZnS QDs. The absorption spectra of CuInS₂-FePt mixed colloids with different concentrations of FePt MNs in chloroform are seen in Fig. S2†. No new band is observed in the absorption spectra of the CuInS₂ QDs after FePt

MNs added into the QD solution. However, a gradual decrease in PL intensity is observed for the blend films with addition of FePt MNs, accompanying by a continuous blue shift of about 15-20 nm in PL peak, as shown in Fig. 4. For example, the PL peak of QD2 is 685 nm and that of the QD2-FePt blend films (FePt/QD2 ratio of 2.0) shifts to 667 nm. Previous studies have reported the PL quenching in the following hybrid nanocrystals. Zhu and his colleagues observed the significant PL quenching in magnetic-fluorescent nanocomposites based on MnFe₂O₄ MNs and CuInS₂/ZnS QDs.²⁴ They suggested that the PL quenching resulted from the effect of MnFe₂O₄ absorption on the QDs emission, or caused by the blocking of MnFe₂O₄ on QDs excitation/emission surfaces. Our previous work also found obvious PL quenching with a red shift in PL peak in CdTe/CdS core/shell QDs when ZnO nanocrystals were added into QDs solution.²⁵ The PL red-shift was considered to result from Förster energy transfer from CdTe/CdS core/shell QDs with a small core to the QDs with a large core. However, the blue-shift of PL in our

CuInS₂ QD-FePt MN blend system is not understood.

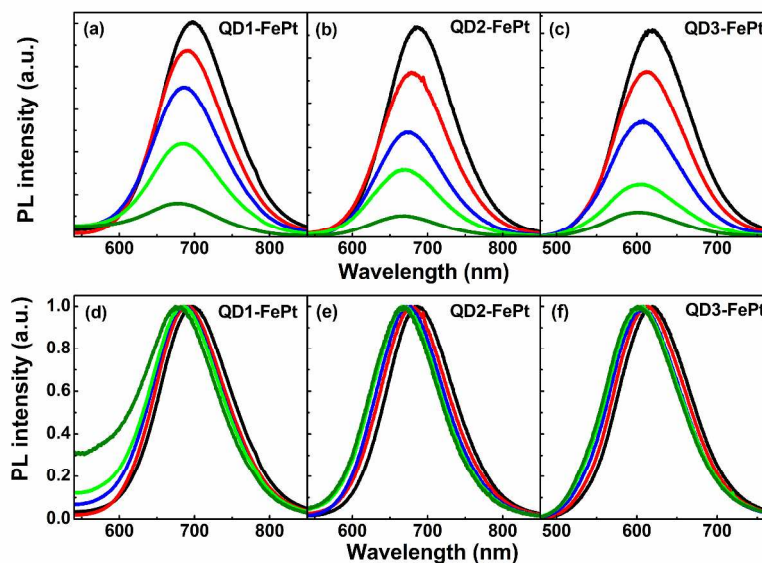


Fig. 4 PL (top) and normalized PL spectra (bottom) of the QDn (n=1-3) before and after addition of FePt MNs with different concentration. Excitation wavelength is 390 nm. The black, red, blue, green, and deep green lines represent the PL spectra of the CuInS₂ QDs in CuInS₂-FePt blend films with FePt/CuInS₂ ratios of 0.0, 0.2, 0.5, 1.0, and 2.0, respectively.

To further determine the mechanism of PL quenching, the PL decays of CuInS₂ QDs were measured in the CuInS₂ QD-FePt MN blend films. Fig. 5 shows the PL decay curves of CuInS₂ QDs in the blend films with different concentrations of FePt MNs under the excitation wavelength of 405 nm. It is clearly shown that the PL decay significantly becomes faster after addition of the FePt MNs. Because the PL decay of the CuInS₂ QDs film was independent on the solution concentration due to close-packed QDs in the thin films [Fig. S3†], the significant decrease in PL decay lifetime was resulted from the adding of FePt MNs.

In general, the shorten PL lifetime can result from energy transfer, electron transfer and nonluminescent exciplex formation²⁶. As seen from Fig.1 and Fig. S2†, there is no spectral overlap between the absorption of FePt MNs and the PL emission of the CuInS₂ QDs, which is a prerequisite for energy transfer, indicating that we can also rule out energy transfer between CuInS₂ and FePt. Thus we can also exclude that the PL quenching arise from exciplex formation because no new absorption band is observed in the absorption spectra of CuInS₂-FePt blend films. Therefore, we suggest that the PL reduction in CuInS₂-FePt blend films originates from electron transfer between CuInS₂ and FePt, because the electron transfer process is an additional nonradiative de-excitation path.²⁷

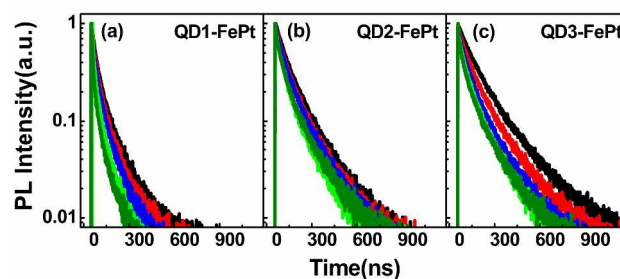


Fig. 5 PL decay curves of the QDn (n=1-3) before and after addition of FePt MNs with different concentration. Excitation wavelength is 405 nm. The black, red, blue, green, and deep green lines represent the PL decay of the CuInS₂ QDs in CuInS₂-FePt blend films with FePt/CuInS₂ ratios of 0, 0.2, 0.5, 1.0, and 2.0, respectively.

The PL decays of QDn-FePt blend films are well fitted by a biexponential function:^{18, 28} $I(t) = A_1 \exp(-t/\tau_1) + A_2 \exp(-t/\tau_2)$, where A_1 and A_2 are fractional contributions of PL decay lifetimes τ_1 and τ_2 . The amplitude-weighted average lifetime τ_{AV} can be obtained by an relation: $\tau_{AV} = (A_1 \tau_1^2 + A_2 \tau_2^2) / (A_1 \tau_1 + A_2 \tau_2)$, the corresponding fitting parameters are summarized in table S2†. The PL dynamics process retains biexponential character, which indicates that the PL in the ZnS shell coated CuInS₂ QDs may come from two channels as follows: the short-lived component τ_1 in tens of nanoseconds may come from a quantized electron state to a deeply-trapped hole state, while the long-lived one τ_2 in hundreds of nanoseconds would result from the defect-related recombination including the recombination from defects/traps formed at the interface between the CuInS₂ core and ZnS shell due to the lattice mismatch and interfacial strain,²⁹ and the donor-acceptor pairs recombination from internal defects.

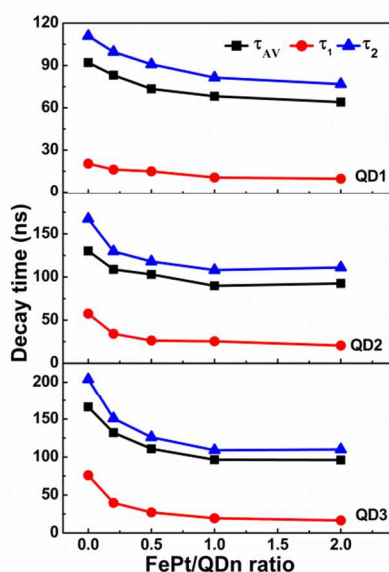


Fig. 6 Fitting parameters τ_1 , τ_2 , and τ_{AV} for CuInS₂ QDs in CuInS₂-FePt blend films as a function of the FePt MN concentration. The black (solid squares), red (solid circles), and blue (solid uptriangles) lines represent the average lifetime τ_{AV} and the components τ_1 , τ_2 of CuInS₂ QDs, respectively.

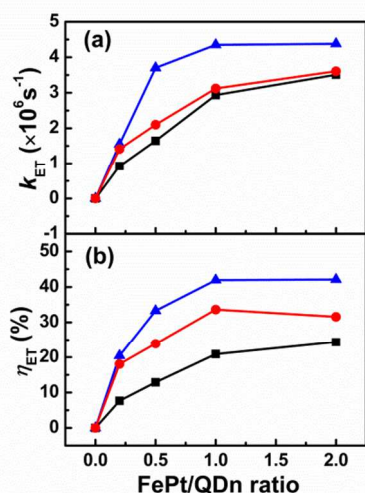


Fig. 7 Electron transfer rate k_{ET} (a) and efficiency η_{ET} (b) for CuInS₂ QD-FePt MN blend films as a function of the FePt MN concentration. The black (solid squares), red (solid circles), and blue (solid uptriangle) lines represent the k_{ET} and η_{ET} of the QD1, QD2, and QD3 blend films with FePt MNs, respectively.

Fig. 6 shows the lifetime components τ_1 , τ_2 , and average lifetime τ_{AV} of the CuInS₂ QDs in CuInS₂-FePt blend films as a function of the FePt MNs concentration. It can be seen that the components τ_1 and τ_2 of PL lifetimes gradually decrease with addition of FePt MNs, and the value of τ_1 is more affected than that of τ_2 after the addition of FePt MNs. The electron transfer rate k_{ET} and efficiency η_{ET} between CuInS₂ QDs and FePt MNs are obtained by expressions: $k_{ET} = 1/\tau_{QD-FePt} - 1/\tau_{QD}$ and $\eta_{ET} = 1 - \tau_{QD-FePt}/\tau_{QD}$, respectively, where the $\tau_{QD-FePt}$ and τ_{QD} are the PL lifetimes of CuInS₂ QDs in blend and neat films. The electron transfer rate k_{ET} and efficiency η_{ET} for QD1-QD3 to FePt MNs as

a function of the FePt MNs concentration are shown in Fig. 7. It can be found that the electron transfer rate k_{ET} increase from 0.92×10^6 , 1.41×10^6 , and 1.55×10^6 s⁻¹ to 3.48×10^6 , 3.61×10^6 and 4.41×10^6 s⁻¹ for QD1-FePt, QD2-FePt, and QD3-FePt systems, respectively, when the FePt/QDn ratio increases from 0.2 to 2.0. The values of k_{ET} is slightly smaller than the ET rate $\sim 10^7$ s⁻¹ of CuInS₂ core-TiO₂ system reported by Sun et al.³¹ This is because the ZnS shell on CuInS₂ acts as a tunneling barrier and the electrons have to tunnel through the shell barrier and transfer to FePt MNs in CuInS₂/ZnS-FePt systems. The electron-transfer processes between QDs and metal oxides/metallic domains were discussed by Kamat for CdSe/TiO₂³² and Sapra for CdSe/Au systems.³³ It has been found that the driving force for electron transfer is provided by the energy difference between the donor (CdSe) and acceptor (TiO₂ or Au) and the electron transfer rate will increase with increasing the energy difference. In our system, high-energy value of the conduction band of CuInS₂ QDs provides favorable conditions to transfer the photoexcited electrons from CuInS₂ QDs to FePt MNs, assigned as transfer channel ET1. However, we also observed another transfer channel ET2, namely, that electrons trapped at donor defects including deep and shallow defects or localized states can also transfer to FePt MNs. The two transfer processes of electrons from CuInS₂ QDs to FePt MNs might cause the PL blue-shift. When the concentration of FePt MNs is low in CuInS₂-FePt blend films and most of CuInS₂ QDs are far from the FePt MNs surface, the PL decay time of the CuInS₂ QDs slightly decreases and the electron transfer rate k_{ET} is low. With further increasing the concentration of FePt MNs, the PL decay time of the CuInS₂ QDs significantly decreases and the rate significantly increases because most of the CuInS₂ QDs distributed near the surface of FePt MNs, as shown in Fig. S1†. In addition, the similar trend of the electron transfer efficiency η_{ET} with the FePt the MN concentration also can be observed. The maximum η_{ET} from QD1-QD3 to FePt MNs is 24%, 33%, and 42%, respectively, when the FePt/QD concentration ratio is 2.0. The results indicate that the PL property of magnetic-fluorescent composites can be tuned by adjusting the distance between CuInS₂ QDs and FePt MNs.

Further we notice that the values of k_{ET} and η_{ET} for CuInS₂-FePt blend films increase clearly as the Cu/In ratio decreases as seen in Fig. 7. It is well accepted that the PL emission from the radiative recombination in CuInS₂ QDs is associated with copper vacancies (V_{Cu}).³⁴ The degree of Cu deficiency in CuInS₂ QDs can result in a reduction in energy level of the valence band and, consequently, a higher band gap is obtained for more Cu-deficient CuInS₂ QDs by virtue of the attenuated repulsion between Cu *d* and S *p* orbitals,^{35,36} which causes the PL blue-shift with decreasing Cu contents. Moreover, the CuInS₂ QDs would have more defect states in the interior of the QDs with decreasing Cu/In molar ratio, which may result in more efficient electron transfer from CuInS₂ QDs to FePt MNs. Based on above results, we proposed a schematic diagram as shown in Fig. 8, to describe the PL recombination and electron transfer processes in CuInS₂ QD-FePt MN blend films.

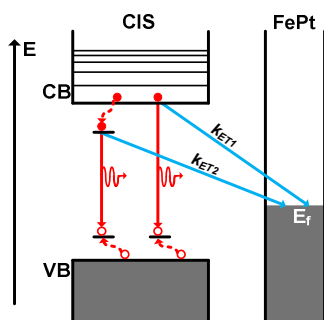


Fig. 8 A schematic diagram of the PL recombination and electron transfer processes in CuInS₂-FePt blend films. ET1 and ET2 represent the transfer channels for electrons from the conduction band (CB) and the defects of CuInS₂ QDs to the Fermi level of the FePt MNs.

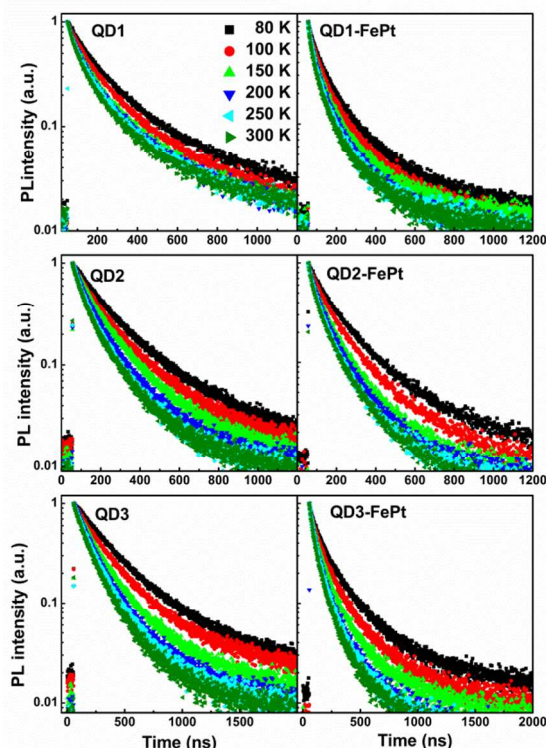


Fig. 9 Temperature-dependent PL decay curves of QDn and QDn-FePt blend films from 80 to 300 K.

Temperature dependence of electron transfer process can give additional information regarding their mechanism. The temperature-related PL decay curves for CuInS₂ QDs films and CuInS₂ QD-FePt MN blend films (FePt/CuInS₂ ratio of 0.5) in the temperature range from 80 to 300 K are shown in Fig. 9. The PL decay curves were analyzed by a biexponential function and the average lifetimes τ_{AV} were obtained. Fig. S4† shows the τ_{AV} of QDn and QDn-FePt blend films ($n=1, 2, 3$) as a function of the temperature. It can be seen that the PL lifetimes of three QDn and QDn-FePt blend films exhibit the similar trend, namely, the PL lifetimes decrease with increasing temperature from 80 to 300 K. It is known that the temperature-dependent PL spectroscopy is often used to study the radiative and nonradiative relaxation processes as well as exciton-phonon coupling in colloidal QDs.^{37, 38} In general, the thermal quenching behavior in QDs is attributed

to multiphonon relaxation and thermally activated nonradiative recombination process.^{39, 40} The thermally activated nonradiative recombination process induces the PL quenching by thermal escape of carrier from luminescent centers. For QDs, this process is generally viewed as escape of thermally activated carriers to trap states.⁴¹ Thus, the decrease of PL lifetime demonstrates that the CuInS₂/ZnS QDs in neat and blend films have some nonradiative trap states on the surface of the QDs or at the interface between the CuInS₂ core and ZnS shell.

Based on the obtained average lifetimes τ_{AV} at various temperatures, we calculate the electron transfer rate k_{ET} and plot the logarithm of the k_{ET} as a function of inverse temperature as shown in Fig. 10. The k_{ET} rates for three CuInS₂-FePt blend films increase with increasing temperature. The k_{ET} rates as a function of temperature can be fitted well with a linear form, indicating that the data follow Arrhenius behavior and the electron transfer can be modeled using the expression:⁴² $k_{ET}=k_0v\exp(-\Delta G/k_B T)$, where ΔG is the Gibbs free energy of activation, k_0 is the electronic transmission coefficient, v is the frequency of nuclear motion over the barrier, T is the temperature, and k_B is the Boltzmann constant. A linear regression of the data gives $\Delta G = 3.24, 3.09, \text{ and } 2.65 \text{ meV}$ for QD1-FePt, QD2-FePt and QD3-FePt system, respectively. The calculated energy of activation slightly decreases with decreasing Cu content in CuInS₂ QDs. The k_{ET} rate shows an Arrhenius dependence on temperature, in agreement with the Marcus theory.^{43, 44} The temperature dependence of k_{ET} rate in CuInS₂-FePt systems shows the same trend as that of CdSe-TiO₂ systems reported by Tafen et al.⁴² However, it has not been reported yet about the temperature dependence of the electron transfer rate between QDs and MNs in experiment. We will study the variation of electron transfer rate between CuInS₂ QDs and FePt MNs with different particle size in detail. Therefore, the result further confirms that the PL quenching mechanism of CuInS₂ QDs in CuInS₂ QD-FePt MN blend films is related to electron transfer.

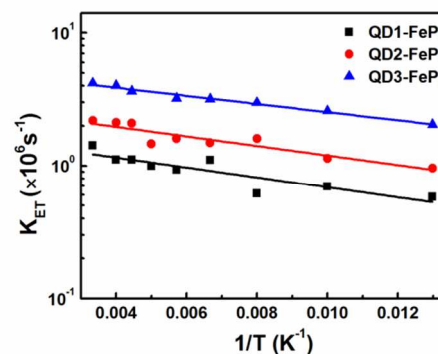


Fig. 10 Electron transfer rate k_{ET} in the CuInS₂ QD-FePt MN blend films as a function of temperature.

Conclusions

We have studied electron transfer-induced PL quenching between CuInS₂ QDs and FePt MNs in their composites by steady-state and time-resolved PL spectroscopy. CuInS₂ QDs coated with ZnS shell having different Cu/In molar ratio exhibited tunable PL peak from 680 to 610 nm. The obvious decrease in both PL intensity and lifetime of CuInS₂ QDs blend films with addition of

FePt MNs demonstrated an electron transfer process occurred from electrons at quantized states in the conduction band of CuInS₂ QDs and the localized defects/traps states of CuInS₂ QDs to FePt MNs. Moreover, the electron transfer rate was found to increase significantly not only with increasing the concentration ratio of FePt MNs to CuInS₂ QDs, but also with increasing the temperature in the range of 80-300 K. These results provide basic physical knowledge to suppression of the PL quenching in CuInS₂ QD-FePt MN nanocomposites.

10 Acknowledgments

This work was supported by the National Natural Science Foundation of China (Nos. 21371071, 61275047, and 11274304) and the Research Project of Chinese Ministry of Education (No. 213009A).

15 Notes and references

^a Key Laboratory of Functional Materials Physics and Chemistry of the Ministry of Education, Jilin Normal University, Siping 136000, China. E-mail: lihaibo@jlnu.edu.cn; zhaojl@jlnu.edu.cn.

^b State Key Laboratory of Inorganic Synthesis and Preparative Chemistry, College of Chemistry, Jilin University, Changchun 130012, China

† Electronic Supplementary Information (ESI) available: Elemental composition of CuInS₂/ZnS QDs; TEM and AFM images for CuInS₂-FePt dropped films with FePt/QD1 ratio of 0.2(a,c) and 2.0(b,d); Absorption spectra of FePt MNs, CuInS₂/ZnS QDs and CuInS₂-FePt mixed colloids in chloroform with different concentrations; PL decay curves of CuInS₂/ZnS core/shell QD3 with different concentration; Fitting parameters of PL decay curves for QD1-QD3 with different concentration of FePt MNs; Temperature-dependent PL decay times τ_{AV} of QDn and QDn-FePt blend films (n=1, 2, 3) at different temperatures from 80 to 300 K. See DOI: 10.1039/b000000x/

- 1 H. Yan, J. C. Zhang, B. W. Yu and Y. Shen, *Acta Materialia*, 2010, 58, 726-733.
- 2 J. W. Ma, Q. S. Fan, L. H. Wang, N. Q. Jia, Z. D. Gu and H. B. Shen, *Talanta*, 2010, 81, 1162-1169.
- 3 L. Sun, Y. Zang, M. D. Sun, H. G. Wang, X. J. Zhu, S. F. Xu, Q. B. Yang, Y. X. Li and Y. M. Shan, *Journal of Colloid and Interface Science*, 2010, 350, 90-98.
- 4 K. Dohnalova, A. N. Poddubny, A. A. Prokofiev, W. D. A. M. de Boer, C. P. Umesh, J. M. J. Paulusse, H. Zuilhof and T. Gregorkiewicz, *Light Sci Appl*, 2013, 2, e47.
- 5 T. Omata, K. Nose and S. Otsuka-Yao-Matsuo, *Journal of Applied Physics*, 2009, 105, 013106.
- 6 S. L. He, H. W. Zhang, S. Delikanli, Y. L. Qin, M. T. Swihart and H. Zeng, *The Journal of Physical Chemistry C*, 2008, 113, 87-90.
- 7 H. Y. Lin, Y. F. Chen, J. G. Wu, D. I. Wang and C. C. Chen, *Applied Physics Letters*, 2006, 88, 161911.
- 8 J. H. Gao, W. Zhang, P. B. Huang, B. Zhang, X. X. Zhang and B. Xu, *Journal of the American Chemical Society*, 2008, 130, 3710-3711.
- 9 S. Giri, D. Li and W. C. W. Chan, *Chemical Communications*, 2011, 47, 4195-4197.
- 10 T. T. Trinh, D. Mott, N. T. K. Thanh and S. Maenosono, *RSC Advances*, 2011, 1, 100-108.
- 11 M. G. Panthani, T. A. Khan, D. K. Reid, D. J. Hellebusch, M. R. Rasch, J. A. Maynard and B. A. Korgel, *Nano Letters*, 2013, 13, 4294-4298.
- 12 H. Z. Zhong, Z. L. Bai and B. S. Zou, *The Journal of Physical Chemistry Letters*, 2012, 3, 3167-3175.
- 13 T. Pons, E. Pic, N. Lequeux, E. Cassette, L. Bezdetnaya, F. Guillemin, F. Marchal and B. Dubertret, *ACS Nano*, 2010, 4, 2531-2538.
- 14 L. Li, T. J. Daou, I. Texier, T. T. Kim Chi, N. Q. Liem and P. Reiss, *Chemistry of Materials*, 2009, 21, 2422-2429.

- 15 K. T. Yong, I. Roy, R. Hu, H. Ding, H. X. Cai, J. Zhu, X. H. Zhang, E. J. Bergey and P. N. Prasad, *Integrative Biology*, 2010, 2, 121-129.
- 16 J. C. Hsu, C. C. Huang, K. L. Ou, N. Lu, F. D. Mai, J. K. Chen and J. Y. Chang, *Journal of Materials Chemistry*, 2011, 21, 19257-19266.
- 17 Y. Hamanaka, T. Kuzuya, T. Sofue, T. Kino, K. Ito and K. Sumiyama, *Chemical Physics Letters*, 2008, 466, 176-180.
- 18 L. Li, A. Pandey, D. J. Werder, B. P. Khanal, J. M. Pietryga and V. I. Klimov, *Journal of the American Chemical Society*, 2011, 133, 1176-1179.
- 19 B. B. Lin, X. Z. Yao, Y. H. Zhu, J. H. Shen, X. L. Yang, H. L. Jiang and X. Q. Zhang, *New Journal of Chemistry*, 2013, 37, 3076-3083.
- 20 H. McDaniel, N. Fuke, N. S. Makarov, J. M. Pietryga and V. I. Klimov, *Nature Communication*, 2013, 4, 2887.
- 21 D. E. Nam, W. S. Song and H. S. Yang, *Journal of Colloid and Interface Science*, 2011, 361, 491-496.
- 22 J. Zhang, R. G. Xie and W. S. Yang, *Chemistry of Materials*, 2011, 23, 3357-3361.
- 23 R. G. Xie, U. Kolb, J. X. Li, T. Basché and A. Mews, *Journal of the American Chemical Society*, 2005, 127, 7480-7488.
- 24 V. G. Demillo, M. Liao, X. Zhu, D. Redelman, N. G. Publicover and K. W. Hunter Jr, *Colloids and Surfaces A: Physicochemical and Engineering Aspects*, 2015, 464, 134-142.
- 25 A. M. Shi, J. H. Sun, Q. H. Zeng, C. Shao, Z. C. Sun, H. B. Li, X. G. Kong and J. L. Zhao, *Journal of Luminescence*, 2011, 131, 1536-1540.
- 26 X. M. Wen, P. Yu, Y. R. Toh, Y. C. Lee, K. Y. Huang, S. J. Huang, S. Shrestha, G. Conibeer and J. Tang, *Journal of Materials Chemistry C*, 2014, 2, 3826-3834.
- 27 C. Shao, X. Meng, P. Jing, M. Sun, J. Zhao and H. Li, *Journal of Luminescence*, 2013, 142, 196-201.
- 28 Z. S. Luo, H. Zhang, J. Huang and X. H. Zhong, *Journal of Colloid and Interface Science*, 2012, 377, 27-33.
- 29 A. Creti, M. Anni, M. Z. Rossi, G. Lanzani, G. Leo, F. Della Sala, L. Manna and M. Lomascolo, *Physical Review B*, 2005, 72, 125346.
- 30 A. Kongkanand, K. Tvrđy, K. Takechi, M. Kuno and P. V. Kamat, *Journal of the American Chemical Society*, 2008, 130, 4007-4015.
- 31 J. H. Sun, J. L. Zhao and Y. Masumoto, *Applied Physics Letters*, 2013, 102, 053119.
- 32 I. Robel, M. Kuno and P. V. Kamat, *Journal of the American Chemical Society*, 2007, 129, 4136-4137.
- 33 U. Soni, P. Tripathy and S. Sapra, *The Journal of Physical Chemistry Letters*, 2014, 5, 1909-1916.
- 34 B. K. Chen, H. Z. Zhong, W. Q. Zhang, Z. A. Tan, Y. F. Li, C. R. Yu, T. Y. Zhai, Y. Bando, S. Y. Yang and B. S. Zou, *Advanced Functional Materials*, 2012, 22, 2081-2088.
- 35 M. Uehara, K. Watanabe, Y. Tajiri, H. Nakamura and H. Maeda, *The Journal of Chemical Physics*, 2008, 129, 4709.
- 36 Y. K. Kim, S. H. Ahn, K. Chung, Y. S. Cho and C. J. Choi, *Journal of Materials Chemistry*, 2012, 22, 1516-1520.
- 37 G. Morello, M. De Giorgi, S. Kudera, L. Manna, R. Cingolani and M. Anni, *The Journal of Physical Chemistry C*, 2007, 111, 5846-5849.
- 38 A. Al Salman, A. Tortschanoff, M. B. Mohamed, D. Tonti, F. van Mourik and M. Chergui, *Applied Physics Letters*, 2007, 90, 3104.
- 39 W. Chen, F. H. Su, G. H. Li, A. G. Joly, J. O. Malm and J. O. Bovin, *Journal of Applied Physics*, 2002, 92, 1950-1955.
- 40 Y. M. Zhao, C. Riemersma, F. Pietra, R. Koole, C. de Mello Donegá and A. Meijerink, *ACS Nano*, 2012, 6, 9058-9067.
- 41 P. T. Jing, J. J. Zheng, M. Ikezawa, X. Y. Liu, S. Z. Lv, X. G. Kong, J. L. Zhao and Y. Masumoto, *The Journal of Physical Chemistry C*, 2009, 113, 13545-13550.
- 42 D. N. Tafen and O. V. Prezhdo, *The Journal of Physical Chemistry C*, 2015, 119, 5639-5647.
- 43 R. A. Marcus and N. Sutin, *Biochimica et Biophysica Acta (BBA) - Reviews on Bioenergetics*, 1985, 811, 265-322.
- 44 K. Tvrđy, P. A. Frantsuzov and P. V. Kamat, *Proceedings of the National Academy of Sciences of the United States of America*, 2011, 108, 29-34.